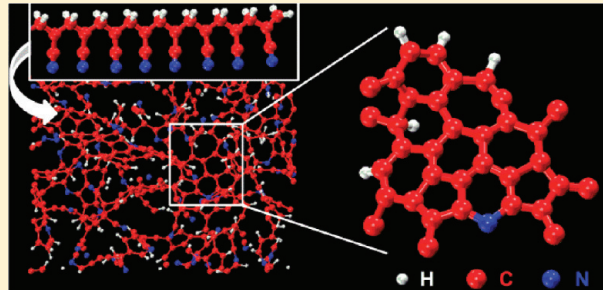


Carbonization in Polyacrylonitrile (PAN) Based Carbon Fibers Studied by ReaxFF Molecular Dynamics Simulations

Biswajit Saha and George C. Schatz*

Department of Chemistry, Northwestern University, Evanston, Illinois 60208, United States

ABSTRACT: The carbonization mechanism in polyacrylonitrile (PAN) based carbon nanofibers is studied using ReaxFF molecular dynamics simulations. Simulations are performed at two carbonization temperatures, 2500 and 2800 K, and also at two densities, 1.6 and 2.1 g/cm³, that are relevant to the experimental carbonization conditions. The results are analyzed by examining the evolution of species with time, including carbon-only ring structures and gaseous species. Formation mechanisms are proposed for species like N₂, H₂, NH₃, and HCN and five-, six-, and seven-membered carbon-only rings, along with polycyclic structures. Interestingly, the formation of five-membered rings follows N₂ formation and usually occurs as a precursor to six-membered rings. Elimination mechanisms for the gaseous molecules are found that are in agreement with previously proposed mechanisms; however, alternative mechanisms are also proposed.



1. INTRODUCTION

Polyacrylonitrile (PAN) based carbon fibers (CF) occupy a premier position among high-performance fibers for composite

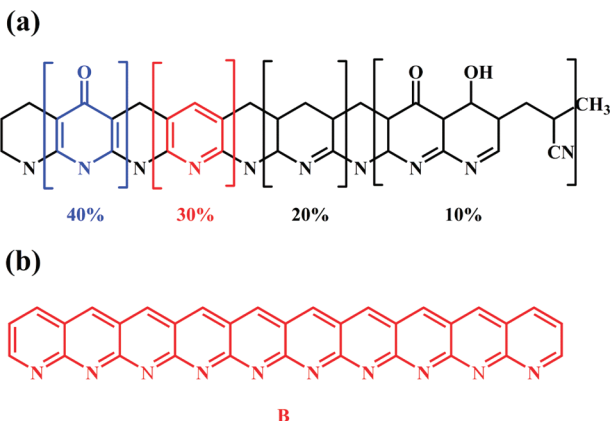


Figure 1. (a) Proposed stabilized PAN from ref 5. (b) Model molecule, denoted B, used in the present study to represent stabilized PAN.

materials, being used as a precursor for about 90% of the carbon fiber production around the world.¹ Carbon fibers have applications in aerospace and sports industries particularly because of their remarkable tensile strength. The preparation of these fibers involves a heat treatment technique to convert a PAN precursor to CF. This is a complex process in which temperature is varied in stages, and oxygen is used in some stages, while emitted gases are removed. Understanding of the oxidative and thermal treatment during this conversion process is crucial to the production of high strength and high modulus fibers; however, only a few scientific studies have been devoted

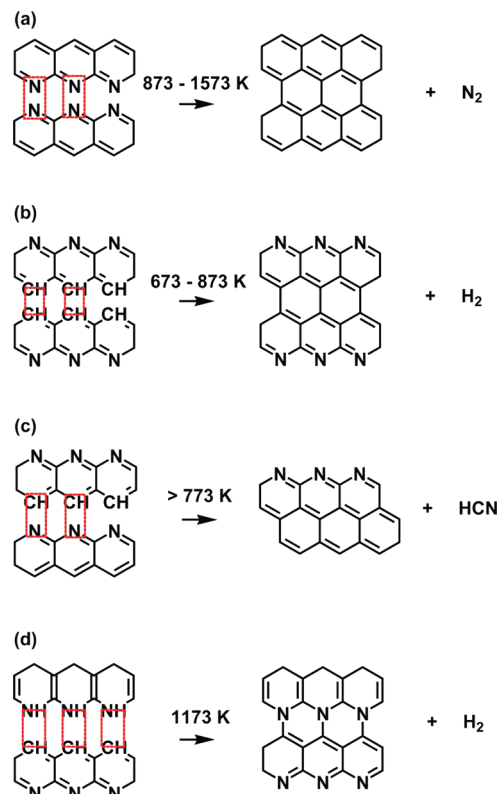


Figure 2. Carbonization mechanisms in PAN, (a) from ref 8 leading to N₂, (b,d) from ref 9 leading to H₂, and (c) from refs 10 and 11 leading to HCN.

Received: January 17, 2012

Revised: March 13, 2012

Published: March 17, 2012



ACS Publications

© 2012 American Chemical Society

4684

dx.doi.org/10.1021/jp300581b | J. Phys. Chem. B 2012, 116, 4684–4692

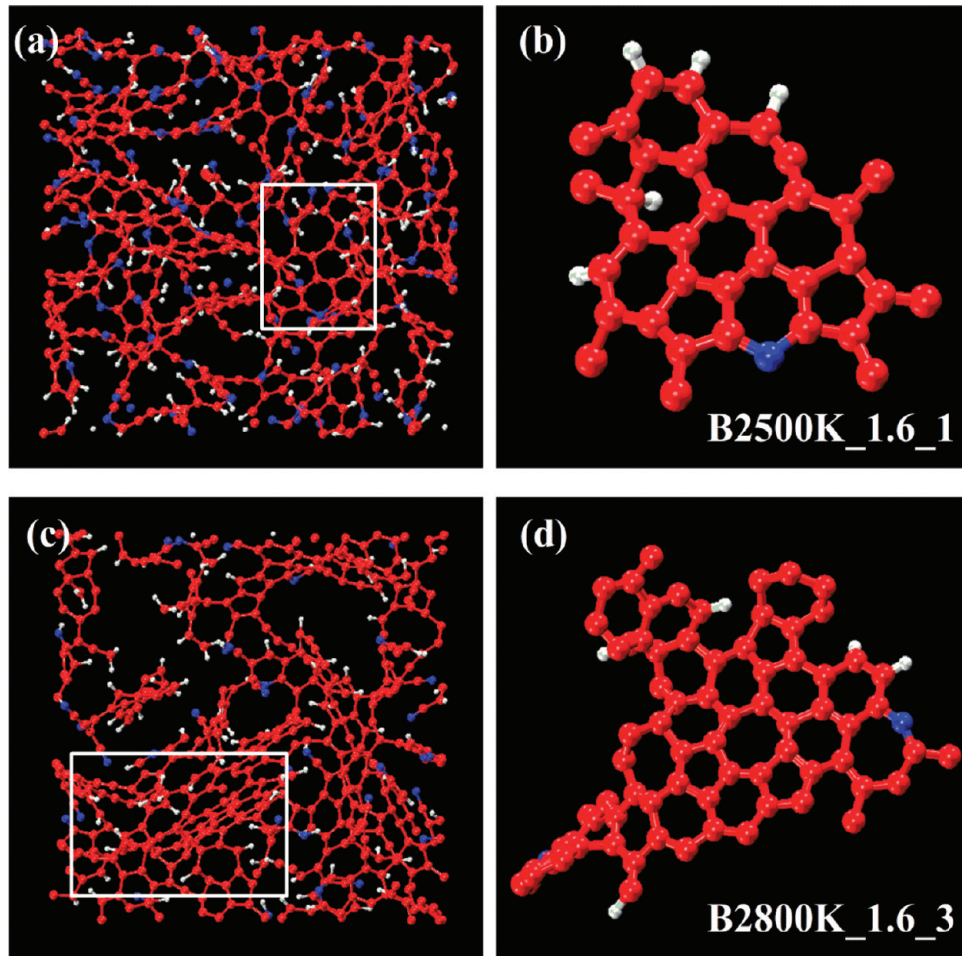


Figure 3. Snapshots at 500 ps from annealing simulations at (a) 2500 K and (c) 2800 K. (b,d) Views of selected parts. Carbon, nitrogen, and hydrogen are represented by red, blue, and white colored spheres, respectively.

to this. Three main stages for the conversion of precursor of the PAN-based fiber to carbon fiber are mentioned in the literature.¹ The first stage involves oxidative stabilization in the temperature range 473–573 K, and there is evidence that ladder structures of heterocyclic six-membered rings form that serve as the precursor to higher temperature processes in the second stage. In the second stage, carbonization in the temperature range ~2000 K occurs in a nitrogen atmosphere in which all heteroatoms are removed as gases such as N₂, H₂, H₂O, NH₃, and HCN, leading to what is termed a turbostratic structure (haphazardly folded carbon sheets). In the third stage, heat treatment up to 2500 K improves the orientation of the basal planes and stiffness of the fibers. Commercially, the stabilization of PAN fibers is done in an oxidizing medium, which is typically air, and it is reported that a polymer backbone containing oxygen-bearing groups that evolves into the PAN ladder structure provides greater stability to sustain the high temperature carbonization treatment.² The mechanism of stabilization is not very clear with some dispute about cross-linking and cyclization. However, cyclization with the formation of six-membered rings seems to have become accepted, though the evidence still remains circumstantial.^{3,4} A scheme for PAN stabilization in air has been proposed in the literature, although the correct structure, in reality, is a more complex three-dimensional structure than is shown in Figure 1a.^{4,5}

Stabilized fibers are heated in order to be carbonized at temperature ~2000 K. During this process, decomposition of the stabilized PAN molecular fragments occurs through primarily intramolecular reactions between functional groups. Intermolecular cross-linking between the fragments also occurs, and overall, the carbonization leads to aromatic rings through dehydration⁶ and elimination reactions of hydrogen cyanide.⁷ Some of the carbonization mechanisms in PAN that have been proposed in the literature on the basis of experimental analysis and that are relevant to our present study are shown in Figure 2. This shows N₂,⁸ H₂,⁹ and HCN elimination^{10,11} mechanisms that have been proposed. Mathematical modeling of the stabilization process of PAN based carbon fibers has been reported,¹² but there is no theoretical/mathematical modeling of the PAN carbonization process so far in the literature. Recently, ReaxFF reactive force field simulations have been performed for the initial stages of phenolic resin carbonization.¹³ These authors reported the formation of small-molecule products such as H₂O, H₂, CO, and C₂H₂ in addition to other species. They proposed an H₂O formation mechanism via β -hydrogen elimination and also found several other pathways for H₂O formation. However, understanding the details of PAN carbonization is not yet very clear, with fundamental questions about how gases form and how six-membered carbon-only rings are formed yet to be determined. Therefore, in this work, we will investigate the carbonization process using

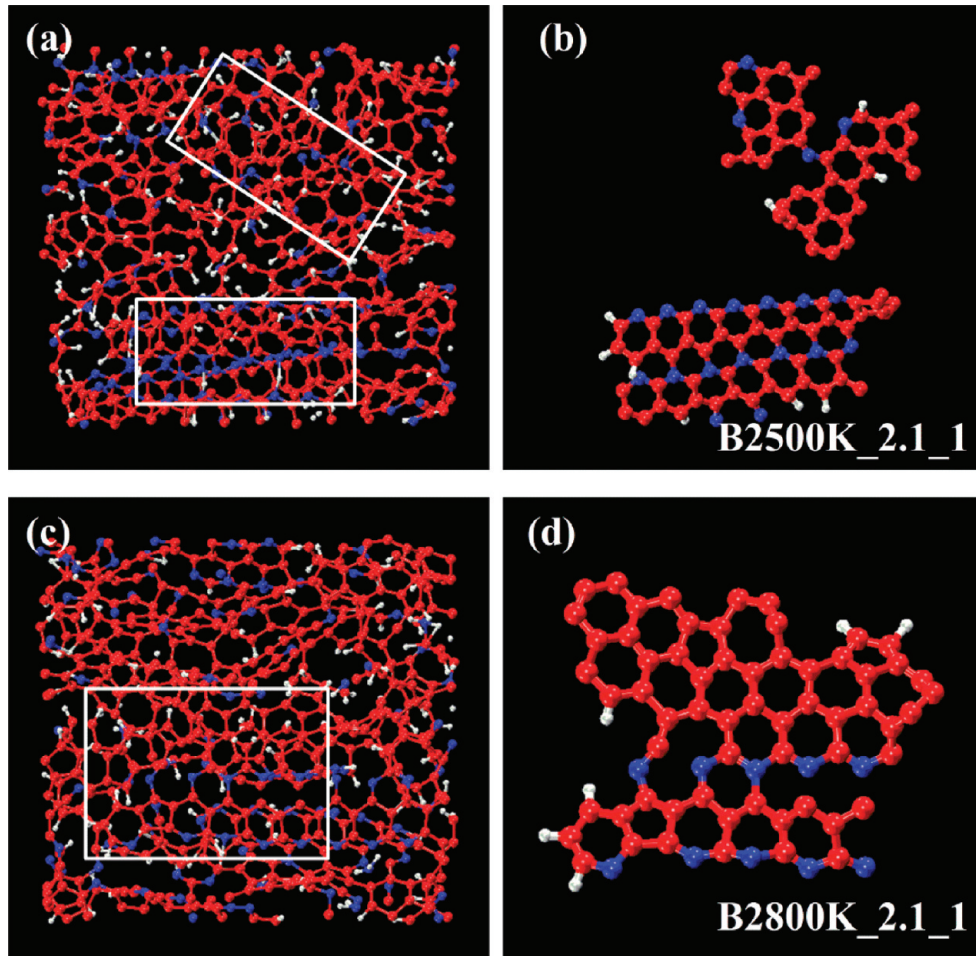


Figure 4. Snapshots at 500 ps from annealing simulations at (a) 2500 K and (c) 2800 K with initial density 2.1 g/cm³. (b,d) Views of selected parts. Carbon, nitrogen, and hydrogen are represented by red, blue, and white colored spheres, respectively.

reactive force field (ReaxFF)¹⁴ molecular dynamics simulations. We will see that these simulations are able to identify reaction mechanisms that lead to the formation of all the gaseous species that are seen in this experiment (here with the restriction that no oxygen is involved), as well as for the formation of five- and six-membered rings and polycyclic structures.

2. REAXFF MOLECULAR DYNAMICS SIMULATIONS

We have investigated the carbonization process using ReaxFF molecular dynamics simulations.¹⁴ ReaxFF uses a general relationship between bond distance and bond order and between bond order and bond energy, leading to proper dissociation of bonds. Other valence terms (angle and torsion) are defined in terms of the same bond orders so that all these terms go to zero smoothly as bonds break. It has been established that the ReaxFF force field is suitable for studying reactions in systems consisting of C, N, O, and H atoms.^{15–20} The accuracy of ReaxFF has been extensively tested for hydrocarbon molecules by considering nonconjugated, conjugated, and radical-containing compounds as described in ref 14. There it was shown that ReaxFF can reproduce the energies associated with the nonreactive and reactive interactions of those compounds. The N–N and N–C–H force field parameters were optimized against DFT calculations and experimental values as described in ref 17. We further calculated the heat of formation for

species relevant to our present study using ReaxFF and compared with experimental values. The ReaxFF heat of formation –12.81 kcal/mol of NH₃ and 37.20 kcal/mol of HCN agree well with experimental values –11.03 and 32.32 kcal/mol, respectively. While this agreement for stable species is very encouraging, we will see later that ReaxFF can be much less accurate for barriers and metastable species. However, at the very high temperatures being considered in these calculations, such errors are likely to be of secondary importance.

One proposal for the structure obtained after stabilization of PAN in air is presented in Figure 1a.^{4,5} Although the correct structure is likely to involve a three-dimensional rather than planar arrangement of the atoms, we will use this as a reference in defining initial conditions. In particular, we consider the molecular structure C₃₂H₁₄N₁₀, shown as molecule B in Figure 1b, as the starting point for our simulations. This is likely to be about 30% of the structure formed during stabilization of PAN, and it has the advantage that only C, N, and H are involved, so that the chemistry is simpler than with structures that also include oxygen, and the ReaxFF force field is better calibrated and validated.¹⁷ Simulations considering other structures as shown in Figure 1a as well as an improved model that includes C, N, H, and O are under consideration. Sixteen B molecules were put in a box to generate a model system for stabilized PAN in our study. Periodic boundary conditions were applied in all the directions of the simulation cell. The size of the simulation cell

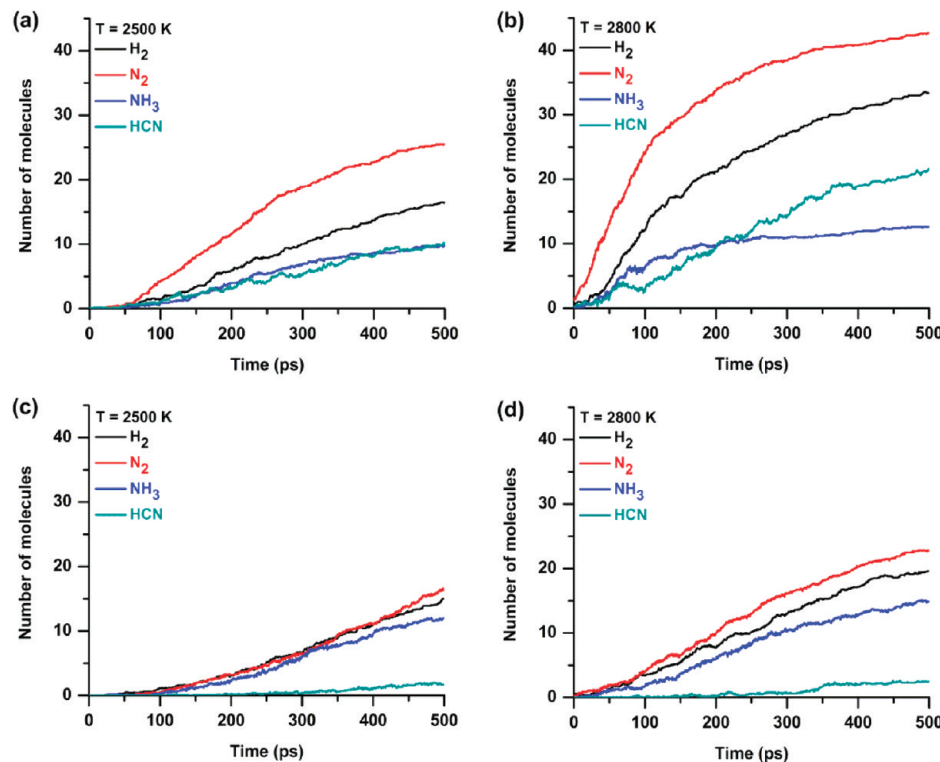


Figure 5. Molecule evolution during annealing simulations at constant temperature. (a,b) Initial density 1.6 g/cm^3 ; (c,d) initial density 2.1 g/cm^3 . Number of molecules averaged over 10 trajectories.

was adjusted such that the initial density was either 1.6 g/cm^3 or 2.1 g/cm^3 at $T = 300 \text{ K}$. These choices of densities are within the reported range found during carbon fiber production from PAN.^{21,22} In an initial calculation, the model systems were equilibrated at 300 K for 60 ps. Ten sample structures were then collected from a 300 K trajectory over a time interval 50 to 60 ps to define initial conditions for the annealing calculations. In the next step, these 10 sample structures were heated to 3000 K at a rate of 10 K/ps. Upon analyzing these 10 trajectories, we found that no reaction or growth was observed until the temperature was raised to 2500 K or beyond. We therefore collected the structures at 2500 and 2800 K and used them for constant temperature simulations in the next stage. These temperatures are somewhat higher than is normally used in the experiments,²³ probably because the short time scale that is feasible for us to simulate necessitates accelerated kinetics. Comparison of results at 2500 and 2800 K will therefore show the sensitivity of the results to this issue. The canonical (NVT molecular dynamics) annealing simulations were performed at constant temperatures 2500 and 2800 K for 500 ps for each trajectory. The temperature was kept constant by employing a Berendsen thermostat with coupling constant 100.0 fs. Including for the initial simulation, the total simulation length of each trajectory was 750 and 780 ps for the 2500 and 2800 K simulations. The trajectories are labeled B2500K_1.6_n and B2800K_1.6_n, where $n = 1$ to 10, for simulations with an initial density 1.6 g/cm^3 , and B2500K_2.1_n and B2800K_2.1_n for simulations with initial density 2.1 g/cm^3 . During the constant temperature simulations, volatile gases such as N_2 , H_2 , HCN , and NH_3 were evolved and removed from the system every 50 ps to simulate what happens during the production of PAN based carbon fiber. The trajectories were analyzed during the course of the annealing simulations by determining the number of species

evolved, the number of ring breaking and formation events, the hybridization types of carbon atoms, the carbon content of the growing structure, elementary reactions that lead to the formation of small species, and the formation and growth mechanism of graphitized carbon structures.

3. RESULTS AND DISCUSSION

For the convenience, we set time $t = 0 \text{ ps}$ when the annealing simulations at constant temperature are started. Therefore, we present results for an annealing simulation of length 500 ps for each temperature. Snapshots of the structures formed at the end of the simulations are shown in Figure 3a,c for simulations at 2500 and 2800 K , respectively, from representative trajectories from the 1.6 g/cm^3 density. Selected parts from these structures, which show graphite-like structures are presented in Figure 3b,d. It is clear from these snapshots that upon annealing at high temperature, the stabilized PAN molecules transform into structures consisting of five-, six- and seven-membered carbon-only rings, while noncarbon atoms are removed to form small molecules such as N_2 , H_2 , HCN , and NH_3 . The presence of five- and seven-membered rings in addition to the more stable six-membered rings is a result of the short length ($<\text{ns}$) of our simulations in comparison with the ($>\text{min}$) time-scale of the experiments,²⁴ and it also reflects the mechanism whereby carbon-only rings are formed, which we will describe later. Figure 3b,d shows that larger polycyclic carbon-only rings are produced in the higher temperature simulations than in the lower temperature simulations. This suggests that the conversion of the five- and seven-membered rings to six-membered rings and larger polycyclic structures will become dominant at longer times in all simulations.

Figure 4 shows snapshots from simulations with initial density 2.1 g/cm^3 . Here, it is noted that, at higher density, more nitrogen

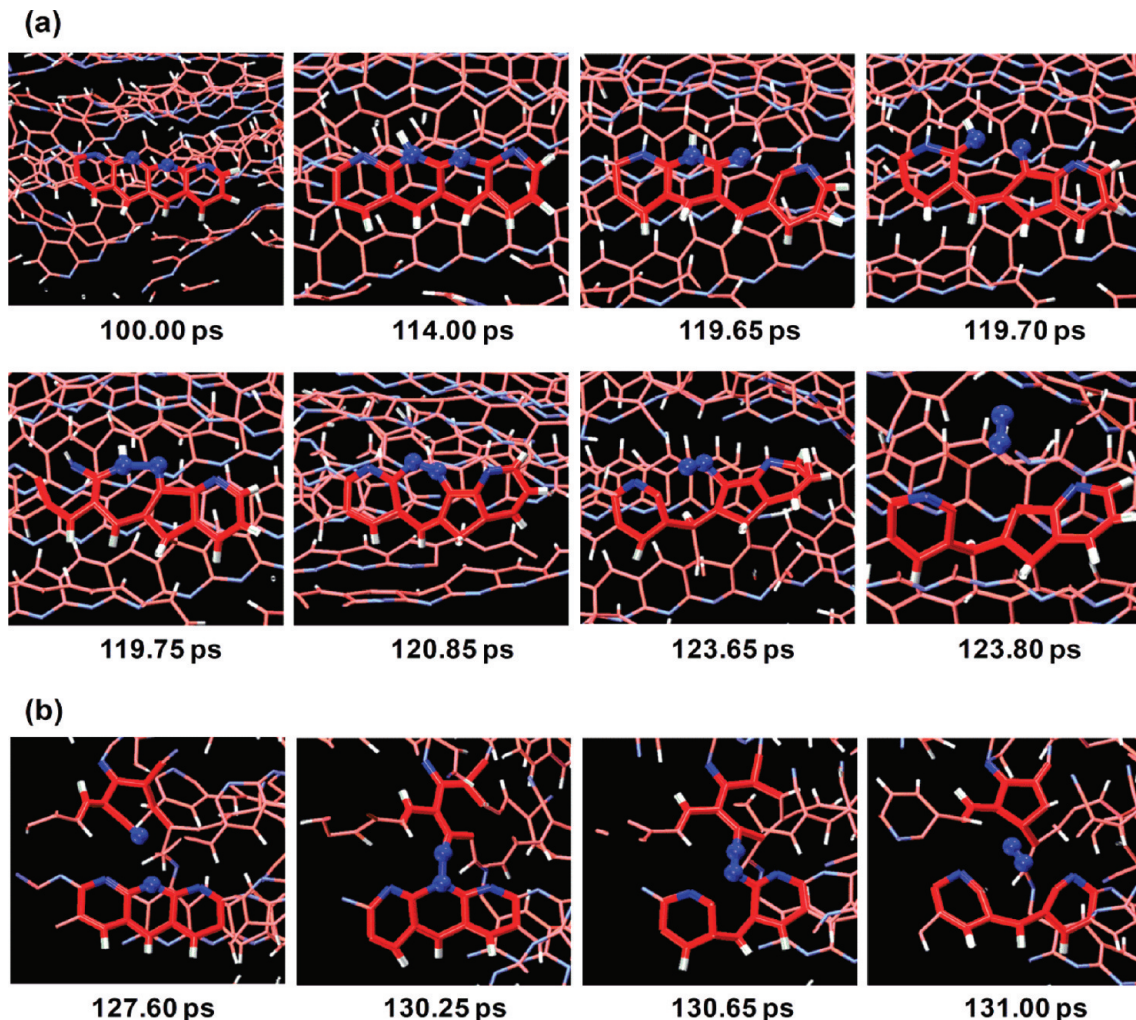


Figure 6. Snapshots showing N_2 formation mechanisms from a representative trajectory, B2500K_1.6_2. Nitrogen atoms are presented by blue colored spheres and other atoms are presented by lines for clarity.

is present in the growing structure. This reflects changes in reaction mechanisms that are described below, but we note that, with continuous annealing at high temperature, the nitrogen content will decrease in the growing structure at all densities, as is known from experiment.^{21,25}

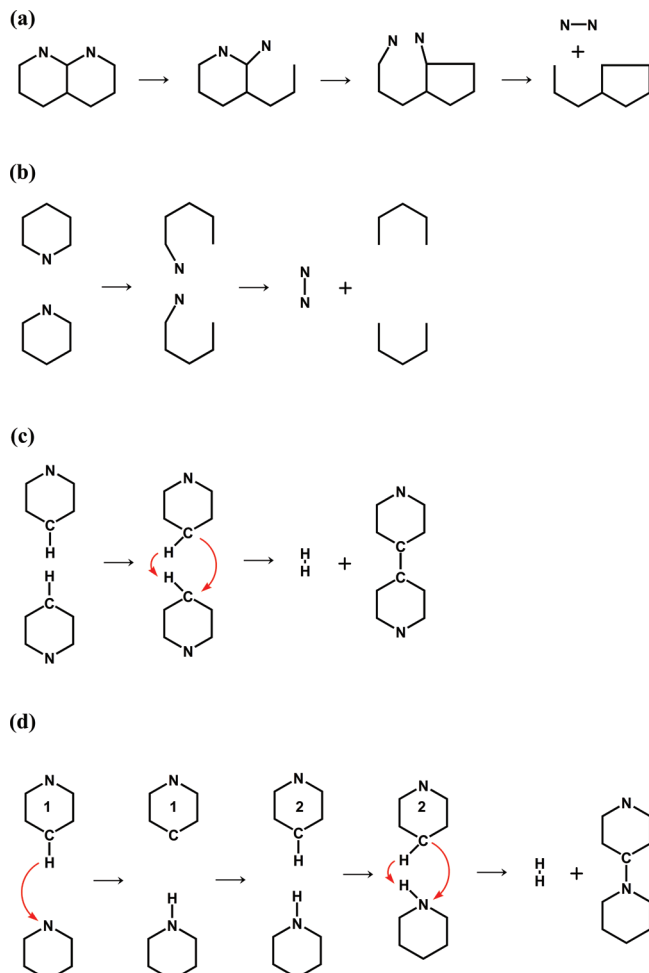
A detailed analysis of the trajectories indicates that the reaction is initiated via radical species formation due to H abstraction. This is in agreement with the thermal decomposition of pyridine as presented in the literature where it is proposed that radical species form as a result of C–H bond fission and subsequent ring-opening.^{26–29} As noted previously, ring breaking starts to occur around $T = 2500$ K and subsequently small molecules, like N_2 , H_2 , HCN , and NH_3 , are formed in addition to other species. As these noncarbon atoms evolve from the system, new π -conjugated graphite-like clusters consisting of five-, six- and seven-membered rings are generated. The formation of C_2H_2 , C_2 or CH_4 is observed occasionally and for short periods of time for the higher temperature simulations. Small species produced during the simulations have been counted and averaged over 10 trajectories as shown in Figure 5. As expected, for the higher temperature of 2800 K, reactions occur more rapidly and a larger number of species are formed compared to the 2500 K simulations. Also, the higher density simulations show a smaller number of species (especially N_2) generated compared to that of the lower density simulations. At higher

density, comparable numbers of H_2 and N_2 are initially formed as is apparent from Figure 5, whereas at lower density, the initial N_2 formation rate is much faster. This is because at higher density initially two B molecules can collide in such a way that H_2 formation is more favorable than N_2 formation. In this case, when two B molecules in the same plane approach each other, new CN-bond formation occurs, and in subsequent steps, H_2 formation occurs. H_2 formation also occurs when two B molecules approach each other and a new CC-bond forms. Therefore, the nitrogen content in the growing structure is larger compared to the low density simulations. Elemental analysis of the largest structures formed in our simulations shows that carbon content is higher in the higher temperature simulations compared to the lower temperature simulations, while the hydrogen and nitrogen content is smaller. This is consistent with experimental observation, which states that carbon content increases, while hydrogen and nitrogen content decreases as carbonization temperature increases.^{21,25}

It is apparent from this figure that, at the lower density, the formation of N_2 and H_2 is more likely than other species and that N_2 formation starts to occur earlier than H_2 formation, whereas in the case of higher density simulations, H_2 formation occurs earlier than N_2 . In these lower density simulations, frequent CN-bond breaking occurs due to thermal decomposition, and N_2 molecules form as illustrated in Figure 6. Here, we have

colored the nitrogen atoms involved in N_2 formation as blue spheres. Two N_2 formation mechanisms, intramolecular and intermolecular, are shown as observed in our simulations. In one case (Figure 6a), the N_2 formation involves nitrogen atoms from the same B molecule. In this case, the CN-bonds of two adjacent pyridine-like six-membered rings on the same B molecule are broken and eventually lead to the formation of a N_2 molecule. In the second case (Figure 6b), N_2 formation involves reaction between two different B molecules. In this case, the CN-bonds of pyridine-like six-membered rings on different B molecules are broken and eventually they encounter each other and N_2 is eliminated. The second mechanism is in agreement with literature proposals⁸ as shown in Figure 2a, but the first one has not previously been considered. In general, N_2 formation occurs in four distinct stages as observed in these simulations: (i) radical species formation due to H-abstraction (ii) CN-bond breaking, pyridine-like six-membered rings of the stabilized PAN molecules break, (iii) NN-bond formation, N with a dangling bond reacts with another nearby N, and finally (iv) subsequent CN-bond breaking leads to N_2 elimination. These stages are shown schematically in Scheme 1a,b. In this

Scheme 1. N_2 and H_2 Elimination Mechanism Observed in the Simulations^a



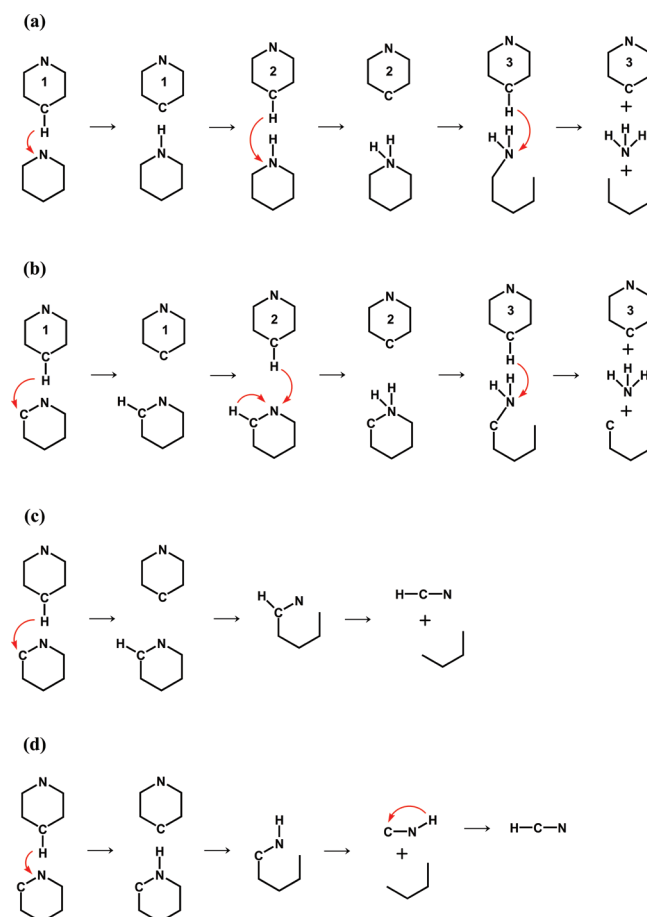
^aConnectivity between two atoms is shown but not the bonding nature. The numbers assigned to the ring structures correspond to the structures (three different units) from which subsequent H abstractions occur.

scheme, the connectivity between atoms is shown, not their bonding nature.

The carbon content in the growing structure is increased as dehydrogenation occurs. H_2 elimination mechanisms observed in these simulations are presented schematically in Scheme 1c,d. Scheme 1c shows H_2 formation when two CH bonds break. In this case, cross-linking between two structures occurs due to formation of a CC bond. This is in agreement with a mechanism proposed in the literature.⁹ Scheme 1d shows an alternative mechanism for H_2 elimination. In this case, in the first step, H is abstracted from a benzene-like structure on one unit by a pyridine-like structure on other unit. Then H_2 formation occurs due to breaking of CH and NH bonds. In this case, cross-linking between two units occurs due to formation of a CN bond. This mechanism is also in conformity with a mechanism proposed in the literature.⁹

NH_3 elimination occurs by a sequence of H abstraction and NH bond formation steps. Two mechanisms are shown in Scheme 2a,b. In these schemes, the numbers assigned to the

Scheme 2. NH_3 and HCN Elimination Mechanism Observed in the Simulation^a



^aConnectivity between two atoms is shown but not the bonding nature. The numbers assigned to the ring structures correspond to the structures (three different units) from which subsequent H abstractions occur. Arrow denotes atoms involved in new bond formation.

benzene-like structures correspond to the structures (three different units) from which subsequent H abstractions occur. The second mechanism is different from the first one only in the first H abstraction step. In the second case, a CH bond is formed instead of a NH bond in the first step. Usually, the CN bond breaks when two NH bonds are formed. Finally, in the

last step, the N atom acquires another H and the CN bond breaks to release NH₃. Scheme 2c,d shows mechanisms for HCN elimination. HCN eliminated via subsequent CN and CC bond breaking is shown in Scheme 2c. In Scheme 2d, CNH is formed first, which then isomerizes to HCN.

The validity of ReaxFF for the CNH → HCN isomerization was checked by performing DFT calculations. DFT(B3LYP/6-311G(2d,2p)) calculations were performed using the Q-Chem package,³⁰ and the results are consistent with literature results.³¹ The ReaxFF activation barrier was calculated by using the geometries of reactant, transition state, and product that were obtained from DFT calculations. The activation barrier is found to be 6.3 and 32.9 kcal/mol at the ReaxFF and DFT levels, respectively, and the exothermicity is -28.7 kcal/mol and -14.6 kcal/mol. Although the ReaxFF and DFT values differ significantly, at least the same trends are found. However, it is clear from this analysis that the conversion of HNC to HCN will not be accurately described. This suggests that the ReaxFF description of nitrogen chemistry could be improved by including non-classical species like CNH and the HCN/CNH isomerization reaction barrier in the parameter training.

The carbon content in the growing structures increases as noncarbon atoms are eliminated in the form of small volatile molecules as described above. This elimination of noncarbon atoms leads to the formation of sp-type (polyyne) carbon chains that can easily form five- or six-membered rings or they can insert into other rings to make more complex polycyclic structures. The formation rates of small molecules are shown in Table 1. The HCN formation rate for high density simulations is very low (around 1/5 of low density simulations), and the N₂ formation rate is almost half of the corresponding rate of the

Table 1. Species Evolution Rate (number of molecules/ns) Averaged over 10 Trajectories

density	1.6 g/cm ³		2.1 g/cm ³		
	temperature	2500 K	2800 K	2500 K	2800 K
N ₂		51.0	85.2	32.8	45.6
H ₂		33.0	66.8	30.0	39.2
HCN		20.4	43.2	3.4	5.0
NH ₃		19.6	25.2	24.0	29.8

low density simulations. The NH₃ formation rates do not differ much for the two temperature simulations.

The newly formed rings consisting of only carbon atoms were counted and are shown in Figure 7. In general, five-membered ring formation occurred first as N₂ formation typically converts a six-membered nitrogen-containing ring of the seed molecules into a five-membered all-carbon chain, and then this becomes a five-membered ring. Initially, five-membered ring formation is prominent for the low density simulations, followed by conversion to six-membered (and occasionally seven) rings through chain insertion and carbon elimination. The formation rate of new rings consisting of carbon atoms only are shown in Table 2.

Table 2. New Ring (Consisting of Carbon Atoms Only) Formation Rate (number of rings/ns) Averaged over 10 Trajectories

density	1.6 g/cm ³		2.1 g/cm ³		
	temperature	2500 K	2800 K	2500 K	2800 K
5-membered ring		57.8	75.2	45.0	55.2
6-membered ring		43.2	89.2	44.0	57.0
7-membered ring		8.6	28.2	10.4	16.8

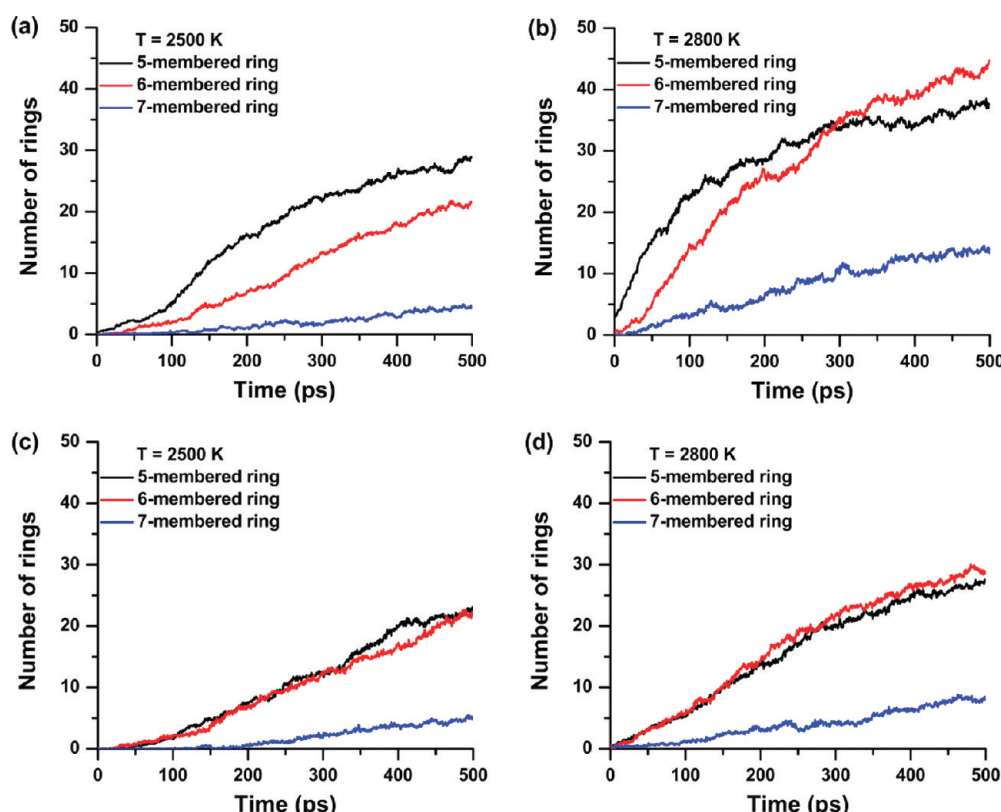


Figure 7. Ring (consisting of C atoms only) formation during annealing simulations at constant temperature. (a,b) Initial density 1.6 g/cm³; (c,d) initial density 2.1 g/cm³. Number of rings averaged over 10 trajectories.

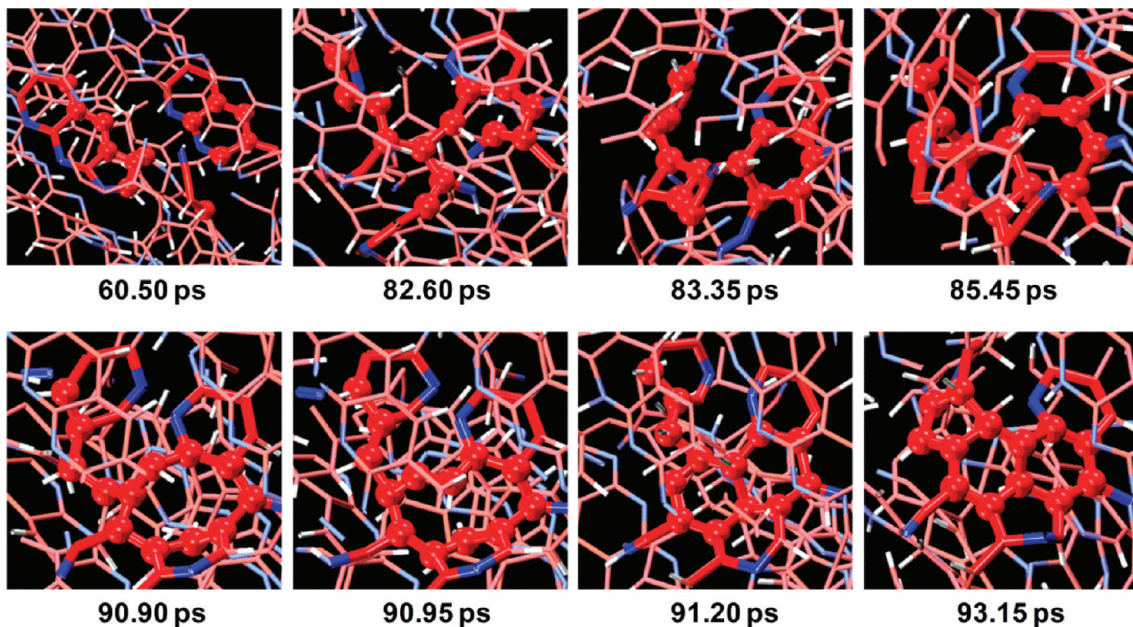


Figure 8. Snapshots showing ring formation and growth mechanisms from a representative trajectory, B2500K_1.6_1. Carbon atoms on rings are presented by red colored spheres and other atoms are presented by lines for clarity.

It is apparent from this table that the formation rate of carbon rings in the 2500 K simulations is the same for both densities, but there are differences at $T = 2800$ K. Thus, as the carbonization temperature increases, the carbon fibers become more graphitic and in agreement with experimental findings.²³

Snapshots from a representative trajectory are shown in Figure 8 showing new carbon-only ring formation and subsequent growth. The parts of the molecules actively taking part in this process are shown in red and carbon atoms are represented by spheres. Other atoms are presented by light colors for clarity. The snapshot at 60.50 ps shows the original structure of the B molecules as well as partly modified structures that take part in the reaction. The snapshot at 82.60 ps shows several CN-bonds breaking and CC-bond formation between two B molecules. This also shows formation of hydrocarbon chain structures. Formation of a six-membered ring is observed at 83.35 ps. A five-membered ring forms at 85.45 ps that is adjacent to this six-membered ring. At 90.90 ps, these five- and six-membered rings merge to form a nine-membered ring. Short carbon-chains, which will supply more carbon atoms to grow this to a larger structure, are attached to this ring. At 90.95 ps, one of these carbon atoms inserts to form a ten-membered ring. This ten-membered ring then transforms into two fused six-membered rings at 91.20 ps. Another five-membered ring forms at 93.15 ps adjacent to one of these six-membered rings. Thus, we see how polycyclic structures are formed around an initial five-membered ring. Larger clusters can also be produced when small clusters merge to form one cluster. Thus, from the present ReaxFF simulations, the following distinct stages are observed in the carbonization mechanism: (i) formation of radical species due to H-abstraction, (ii) formation of polyyne chains via N₂ evolution followed by five- and six-membered ring formation on the same unit, (iii) ring expansion as a result of the condensation of carbon chains that are attached to the initial ring, (iv) ring cluster growth, small clusters on different units react to form larger clusters, while H₂, HCN, NH₃, etc. species are produced. This ultimately leads to the formation of graphitic structures.

4. CONCLUSIONS

ReaxFF molecular dynamics simulations were performed to understand the carbonization mechanism in PAN-based carbon nanofibers. Simulations were performed at two carbonization temperatures, 2500 and 2800 K, and two initial densities, 1.6 and 2.1 g/cm³, and the results are generally consistent. These simulation conditions are based on parameters used in experimental carbonization, although with a somewhat higher temperature that is necessitated by the requirement that the simulations can only be done for subnanosecond time scales. We found that small species like N₂, H₂, HCN, and NH₃ molecules evolve as volatile gas during the carbonization, in agreement with experimental observations, and thus, the carbon content of the materials is gradually increased. In addition five- and six-membered rings are formed, and eventually, these become polycyclic rings. The elimination mechanisms leading to small molecule production are in agreement with previously proposed mechanisms, but additional mechanisms are also found. The mechanisms for forming five-membered rings are found to be coupled to the N₂ formation process, as this leads to polyyne chains that easily cyclize. Thus, we propose that the formation of five-membered rings plays an important role in the initial states of ring growth during carbonization. At higher temperature and also at higher density, the formation of six-membered rings is more prominent compared to lower temperature and density.

The connection of these results to carbonization experiments is entirely qualitative at this point. Such experiments are done over much longer time scales, and an important feature of the carbonization process^{21,24} is that the mechanical properties of the resulting fibers are strongly dependent on the conditions of the stabilization process that precedes carbonization. Also, the rate of increase of temperature in the carbonization step determines the rate at which gases are emitted, and if this is too high, a more defected fiber structure results. These results suggest that additional simulations that study the effect of different choices of the structure produced after stabilization and different carbonization conditions and gas removal schemes will be useful.

AUTHOR INFORMATION

Corresponding Author

*E-mail: g-schatz@northwestern.edu.

Notes

The authors declare no competing financial interest.

ACKNOWLEDGMENTS

We are thankful to Dr. Adri van Duin, Pennsylvania State University, U.S.A., for the use of the ReaxFF program and his help. The Quest computer system at Northwestern University was used for these simulations. This material is based upon work supported by the U.S. Army Research Laboratory and the U.S. Army Research Office under grant number W911NF-09-1-0541.

REFERENCES

- (1) Rahaman, M. S. A.; Ismail, A. F.; Mustafa, A. *Polym. Degrad. Stab.* **2007**, *92*, 1421–1432.
- (2) Rangarajan, P.; Bhanu, V. A.; Godshall, D.; Wikels, G. L.; McGrath, J. E.; Baird, D. G. *Polymer* **2002**, *43*, 2699–2709.
- (3) Bashir, Z. *Carbon* **1991**, *29*, 1081–1090.
- (4) Usami, T.; Itoh, T.; Ohtani, H.; Tsuge, S. *Macromolecules* **1990**, *23*, 2460–2465.
- (5) Morita, K.; Murata, Y.; Ishitani, A.; Muryama, K.; Ono, T.; Nakajima, A. *Pure Appl. Chem.* **1986**, *58*, 455–468.
- (6) Watt, W. *Proc. R. Soc. Lond. Ser. A* **1970**, *319*, 5–15.
- (7) Shionoya, I.; Uchida, T.; Nukada, K. In *Preprints of the International Carbon Conference*, The Arbeitskreis Kohlenstoff of the Deutsche Keramische Gesellschaft, Baden-Baden, Germany, 1972; pp 293–295.
- (8) Watt, W. In *Handbook of Composites, Strong Fibers*; Watt, W., Perov, B. V., Eds.; Elsevier Science: Amsterdam, The Netherlands, 1985; Vol. 1, pp 327–387.
- (9) Watt, W.; Green, J. *International Conference on Carbon Fibres*, London, U.K., 1971.
- (10) Watt, W. *3rd Carbon Conference*, London, U.K., 1970.
- (11) Bailey, J. E.; Clarke, A. J. *Chemistry in Britain* **1970**, *6*, 484–489.
- (12) Dunham, M. G.; Edie, D. D. *Carbon* **1992**, *30*, 435–450.
- (13) De-en, J.; van Duin, A. C. T.; Goddard, W. A.; Dai, S. *J. Phys. Chem. A* **2009**, *113*, 6891–6894.
- (14) van Duin, A. C. T.; Dasgupta, S.; Lorant, F.; Goddard, W. A. *J. Phys. Chem. A* **2001**, *105*, 9396–9409.
- (15) Chenoweth, K.; van Duin, A. C. T.; Goddard, W. A. *J. Phys. Chem. A* **2008**, *112*, 1040–1053.
- (16) Zhang, L.; Zybin, S. V.; van Duin, A. C. T.; Dasgupta, S.; Goddard, W. A. *J. Phys. Chem. A* **2009**, *113*, 10619–10640.
- (17) Kamat, A. M.; van Duin, A. C. T.; Yakovlev, A. *J. Phys. Chem. A* **2010**, *114*, 12561–12572.
- (18) Desai, T. G.; Lawson, J. W.; Kebbinski, P. *Polymer* **2011**, *52*, 577–585.
- (19) Han, S.-P.; van Duin, A. C. T.; Goddard, W. A.; Strachan, A. *J. Phys. Chem. B* **2011**, *115*, 6534–6540.
- (20) Qian, H.-J.; van Duin, A. C. T.; Morokuma, K.; Irle, S. *J. Chem. Theory Comput.* **2011**, *7*, 2040–2048.
- (21) Ko, T.-H. *J. Appl. Polym. Sci.* **1991**, *43*, 589–600.
- (22) Liu, J.; Wang, P. H.; Li, R. Y. *J. Appl. Polym. Sci.* **1994**, *52*, 945–950.
- (23) Zhou, Z.; Lai, C.; Zhang, L.; Qian, Y.; Hou, H.; Reneker, D. H.; Fong, H. *Polymer* **2009**, *50*, 2999–3006.
- (24) Fitzer, E.; Frohs, W.; Heine, M. *Carbon* **1986**, *24*, 287–305.
- (25) Wu, Z.; Pan, D.; Fan, X.; Qian, B. *J. Appl. Polym. Sci.* **1987**, *33*, 2877–2884.
- (26) Morris, V. R.; Bhatia, S. C.; Stelson, A. W.; Hall, J. H. *Energy Fuels* **1991**, *5*, 126–133.
- (27) Ikeda, E.; Mackie, J. C. *J. Anal. Appl. Pyrolysis* **1995**, *34*, 47–63.
- (28) Hore, N. R.; Russell, D. K. *J. Chem. Soc., Perkin Trans. 2* **1998**, *269*–275.
- (29) Ninomiya, Y.; Dong, Z.; Suzuki, Y.; Koketsu, J. *Fuel* **2000**, *79*, 449–457.
- (30) Shao, Y.; Fusti-Molnar, L.; Jung, Y.; Kussmann, J.; Ochsenfeld, C.; Brown, S. T.; Gilbert, A. T. B.; Slipchenko, L. V.; Levchenko, S. V.; O'Neill, D. P.; DiStasio, R. A., Jr.; Lochan, R. C.; Wang, T.; Beran, G. J. O.; Besley, N. A.; Herbert, J. M.; Lin, C. Y.; Voorhis, T. V.; Chien, S. H.; Sodt, A.; Steele, R. P.; Rassolov, V. A.; Maslen, P. E.; Korambath, P. P.; Adamson, R. D.; Austin, B.; Baker, J.; Byrd, E. F. C.; Dachs, H.; Doerkens, R. J.; Dreuw, A.; Dunietz, B. D.; Dutoi, A. D.; Furlani, T. R.; Gwaltney, S. R.; Heyden, A.; Hirata, S.; Hsu, C.-P.; Kedziora, G.; Khaliullin, R. Z.; Klunzinger, P.; Lee, A. M.; Lee, M. S.; Liang, W.; Lotan, I.; Nair, N.; Peters, B.; Proynov, E. I.; Pieniazek, P. A.; Rhee, Y. M.; Ritchie, J.; Rosta, E.; Sherrill, C. D.; Simmonett, A. C.; Subotnik, J. E.; Woodcock, H. L., III; Zhang, W.; Bell, A. T.; Chakraborty, A. K.; Chipman, D. M.; Keil, F. J.; Warshel, A.; Hehre, W. J.; Schaefer, H. F., III; Kong, J.; Krylov, A. I.; Gill, P. M. W.; Head-Gordon, M.; Gan, Z.; Zhao, Y.; Schultz, N. E.; Truhlar, D.; Epifanovsky, E.; Oana, M. *Q-Chem*, version 3.1; Q-Chem, Inc.: Pittsburgh, PA, 2007.
- (31) Jursic, B. S. *Chem. Phys. Lett.* **1996**, *256*, 213–219.